JOURNAL OF SOLID STATE CHEMISTRY 119, 50–61 (1995)

Structural, Magnetic, and EPR Studies of $BaCuO_{2+x}$

N. Guskos,[1] V. Likodimos, and C. A. Londos

Solid State Section, Department of Physics, University of Athens, Panepistimiopolis, GR-15784 Zografou, Athens, Greece

V. Psycharis, C. Mitros, A. Koufoudakis, and H. Gamari-Seale

Institute of Material Science, N.C.S.R. "Demokritos," Ag. Paraskevi Attikis, GR-15310, Athens, Greece

and

W. Windsch and H. Metz

Fachbereich Physik, Universitat Leipzig, Linnestr. 5, 0-7010 Leipzig, Germany

Received June 20, 1994; in revised form March 20, 1995; accepted March 23, 1995

XRD, magnetic susceptibility, and EPR studies are reported for the $BaCuO_{2+x}$ compound in both the oxygenated and nonoxygenated phases. The XRD analysis has shown essential differences in the disordered part between the oxygenated and the nonoxygenated samples. The magnetic susceptibility measurements have shown strong ferromagnetic intracluster interactions among copper ions in the ordered part of the compound. At low temperature, antiferromagnetic intercluster interactions mediated by the disordered part predominate. EPR measurements in both phases have revealed a spectrum of Cu^{2+} ions, in orthorhombic local symmetry, which is attributed to copper ions in the disordered part. An intense exchange-narrowed EPR line has also been observed in both phases, which is ascribed to the copper clusters in the ordered part. The temperature dependence of the intensity and linewidth of this line is consistent with the bulk magnetic behaviour. At low temperature, the divergent behaviour of the EPR parameters indicates that antiferromagnetic ordering may occur. Additionally, it was found that the EPR spectra are essentially influenced by thermal treatment and the ordering of the oxygen atoms in the disordered part of the compound. © 1995 Academic Press, Inc.

1. INTRODUCTION

The barium cuprate compound ($BaCuO_{2+x}$) is usually observed in the preparation of the *RE*123 materials (*RE* = rare earth ions) as a parasitic phase. The compound is nonstoichiometric and its crystal structure exhibits substantial differences depending on the preparation conditions and the oxygen content (1–4). Its presence as an impurity phase was thought to obscure the intrinsic magnetic susceptibility of the Y123 materials (5, 6), while it has a negligible effect on the *RE*123 materials (7). Inclusions of $BaCuO_2$ in the *RE*123 compounds may seriously affect the EPR measurements, especially at low temperatures, and it was suggested that they are responsible for the low-temperature EPR signal observed in the *RE*123 systems, though this assignment is still ambiguous (8, 9). Barium cuprate has also been classified as one of the few copper oxides exhibiting ferromagnetic interactions (10, 11). However, no detailed study of its magnetic behaviour in combination with its complex structural state has been reported so far.

The aim of the present work is to report our structural, magnetic, and EPR studies on barium cuprate compounds with different oxygen contents and subjected to various heat treatments.

2. EXPERIMENTAL RESULTS

Three samples of $BaCuO_{2+x}$ hereafter designated as I, II, and III were prepared by the solid state reaction technique. The samples were fired at 890°C for 6 hr. The annealing process was done in several steps by increasing the temperature at every step, in a flowing oxygen atmosphere, and with intermediate grinding. Sample I was annealed up to 955°C, while samples II and III were annealed up to 1000°C. The step increase of temperature was 15°C for sample II and 10°C for sample III. The duration of each step was 16 hr. The oxygenation of all samples was done at 450°C in a flowing oxygen atmosphere for 24 hr. In order to reduce the oxygen content the samples were annealed at 900°C in flowing He gas for 24 hr. followed by fast cooling to room temperature (RT) in the He atmosphere.

Resistivity measurements were done by the four-points

[1] To whom correspondence should be addressed.

0022-4596/95 $12.00

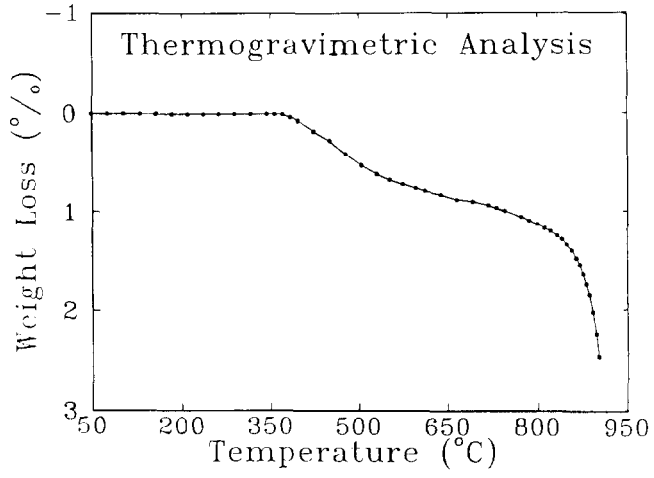

FIG. 1. Oxygen content vs temperature for the oxygenated $BaCuO_{2+x}$ compound.

method on cylindrical-shaped samples from RT to liquid nitrogen temperature (NT). The results indicate a semiconducting behaviour for all samples.

2.1. TGA Measurements

The changes in the oxygen content of the oxygenated samples were monitored by thermogravimetric analysis (TGA). Small amounts of the samples (70–100 mg) were put in a TGA apparatus (Perkin–Elmer TGS-2) under flowing He gas at a rate of 4°C/min in the range 50 to 900°C. The TGA curve for sample I is presented in Fig. 1. No weight loss was observed from RT up to 350°C. Beyond that temperature the sample started losing weight at an almost constant rate. At about 550°C the rate of weight loss decreased and remained constant up to about 800°C. Then, the rate increases sharply up to about 900°C. Above that temperature the samples melted. The weight loss is attributed to oxygen loss, since fully nonoxygenated samples did not give any sign of weight loss in TGA up to about 900°C. The total weight loss was found to be about 2.54%, which amounts to a 0.369 variation of x. The measurements are consistent with previous results (3) and indicate nonstoichiometry of the compound.

2.2. XRD Measurements

X-ray powder diffraction (XRD) data were collected with a D 500 Siemens diffractometer using Cu$K\alpha$ radiation and a graphite crystal monochromator, from 10 to 100° in steps of 0.03° in 2θ. The power conditions were set at 40 kV/35 mA. The aperture slit and the solar slit were set at 1°. In this study the results of the Rietveld refinement (12) for an oxygenated (sample IIIA) and a nonoxygenated (sample IIIB) barium copper oxide with nominal composition $BaCuO_2$ are presented. The final values of the fractional atomic coordinates and the occupancy factors are listed in Table 1. In this table the atoms called A are oxygens in the disordered part of the structure and correspond to the A atoms as reported by Paulus *et al.* (3). By using the ordered part of the structure, which means the atoms Ba1, Ba2, Ba3, Cu1, Cu2, Cu3, O1, O2, O3, and A4 (3), as the starting structural model for the Rietveld programme, the observed structure factors were derived. The SHELX'76 programme was used for difference Fourier map calculations. Initially, the Cu4 and Cu5 atoms were located. With successive Fourier map calculations it was possible to locate the A atoms given by Paulus *et al.* (3). Except for the A1 atom at the origin (0.0, 0.0, 0.0), which corresponds to an electron density of 4 electrons/Å^3, all the other peaks in the Fourier map correspond to an electron density in the range of 1–2 electrons/Å^3, which explains the observed, quite unstable behaviour of these atoms during the refinement with the Rietveld method. With powder XRD data it is difficult to locate chemical elements with low atomic scattering factors, especially in cases where they statistically occupy the corresponding crystallographic sites. Of the 10 atoms called A by Paulus *et al.* (3) we keep in our structural model only A1, A4, A5, A8, A9 (Table 1), for the following reasons: the structural parameters of the A2 (0.0, 0.1687, 0.3529), A3 (0.0446, 0.1037, 0.0), A6 (0.0740, 0.5, 0.5), A7 (0.3654, 0.0, 0.0), A10 (0.0875, 0.5, 0.2824) atoms located by Paulus *et al.* (3) are not refined in their study. The atoms A6 and A10 are very close to A8 and A9, respectively. Their corresponding parameters are highly correlated during the refinement. Therefore only A8 and A9 atoms were included in our structural model. The A2 atom is very close to Ba1 (~0.8 Å) (3) and we consider it a ghost peak. The A3 atom is located in the cavity of the $Cu_{18}O_{24}$ polyhedron, an almost spherical cage with radius 3.7 Å, centered at the origin (see below). We believe that the disordering is not bounded only to the atom at the origin as has been discussed by Weller and Lines (4), but it is more extensive. The A7 atom lies between A4 and Cu4 atoms and very close to them. The positioning of A5, A6, and A8 atoms close to the (0.5, 0.0, 0.0) sites indicates an extremely disordered situation. The A9 atoms are close to the Cu5 sites and for the nonoxygenated sample III its coordinates converge to almost the same x, y, z parameters as for Cu5. For this reason it was excluded from the structural model for the nonoxygenated sample III. From the calculated occupancies (Table 1) the unit cell contents are Ba88 Cu96.8(3) O208(4) and Ba88 Cu97.1(3) O185(3) for the oxygenated and the nonoxygenated sample III, respectively. With $z = 96$ we obtain the formula units (or the contents for the asymmetric unit of the unit cell) $Ba_{0.92}Cu_{1.01}O_{2.17(4)}$ (sample III-A) and $Ba_{0.92}Cu_{1.01}O_{1.93(2)}$ (sample III-B). The final Rietveld refinement patterns for the two samples are shown in Fig. 2.

TABLE 1

Structural Parameters and Agreement Indexes (R Factors) for the Sample IIIA [Produced in Oxydized Atmosphere (First Line)] and Sample IIIB [Produced in Reduced Atmosphere (Second Line)]

Atom	Site	x	y	z	Occupancy
Ba_1	48*j*	0.0000	0.1510(2)	0.3126(1)	1.0
		0.0000	0.1503(1)	0.3102(1)	1.0
Ba_2	24*h*	0.3656(2)	0.0000	0.3656(1)	1.0
		0.3615(1)	0.0000	0.3615(1)	1.0
Ba_3	16*f*	0.1769(1)	0.1769(1)	0.1769(1)	1.0
		0.1781(1)	0.1781(1)	0.1781(1)	1.0
Cu_1	48*i*	0.1502(2)	0.2500	0.3498(2)	1.0
		0.1502(2)	0.2500	0.3498(2)	1.0
Cu_2	24*h*	0.1258(3)	0.0000	0.1258(3)	1.0
		0.1252(2)	0.0000	0.1252(2)	1.0
Cu_3	12*e*	0.2037(6)	0.0000	0.0000	1.0
		0.2049(5)	0.0000	0.0000	1.0
Cu_4	12*e*	0.430(1)	0.0000	0.0000	0.73(2)
		0.4318(8)	0.0000	0.0000	0.79(2)
Cu_5	12*d*	0.2500	0.0000	0.5000	0.33(2)
		0.2500	0.0000	0.5000	0.30(2)
O_1	48*k*	0.072(1)	0.072(1)	0.193(1)	1.0
		0.0710(8)	0.0710(8)	0.190(1)	1.0
O_2	48*k*	0.1467(9)	0.1467(9)	0.338(2)	1.0
		0.1477(7)	0.1477(7)	0.346(1)	1.0
O_3	48*k*	0.264(1)	0.264(1)	0.088(1)	1.0
		0.2673(9)	0.2673(9)	0.083(1)	1.0
A_1	2*a*	0.0000	0.0000	0.0000	0.5(2)
		—	—	—	—
A_4	12*e*	0.333(3)	0.0000	0.0000	1.0
		0.336(2)	0.0000	0.0000	1.0
A_5	6*b*	0.5000	0.0000	0.0000	1.0(1)
		0.5000	0.0000	0.0000	0.7(1)
A_8	48*j*	0.0000	0.094(2)	0.456(2)	0.64(4)
		0.0000	0.093(2)	0.446(4)	0.76(4)
A_9	48*i*	0.055(2)	0.555(2)	0.2500	0.54(4)
		—	—	—	—

Note. Sample IIIA: a = 18.3161 Å, R_p = 6.20, R_{wp} = 5.38, R_B = 5.29, R_{exp} = 3.27. Sample IIIB: a = 18.3054 Å, R_p = 4.43, R_{wp} = 4.37, R_B = 5.16, R_{exp} = 3.28.

The bond lengths for the nonoxygenated and oxygenated sample III are listed in Table 2, together with the value derived in the previous structural studies (1, 2, 3, 4). The bond length values for the nonoxygenated sample III are in better agreement with the results of Gutau and Muller-Buschaum (2) and Paulus *et al.* (3). The part of the structure that has been acurately described in the previous studies concerns the $Cu_{18}O_{24}$ polyhedron (6 Cu3, 12 Cu2, and 24 O1 atoms) around the origin (Fig. 3a) and the six Cu-member ring Cu_6O_{12} polyhedron (6 Cu1, 6 O2 and 6 O3 atoms) around the 8*c* site ($\frac{1}{4}$, $\frac{1}{4}$, $\frac{1}{4}$) (Fig. 3b). The A4 and A9 atoms are located in positions around these polyhedra in such a way as to form square pyramids for Cu3 and Cu1 atoms. The $Cu_{18}O_{24}$ and Cu_6O_{12} polyhedra are connected by the Ba3 atoms which lie in the cavity of nine oxygens forming the polyhedron (BaO_9) shown in Fig. 3c. The above-mentioned polyhedra form the skeleton of the ordered part of the structure and they are extended along the four main diagonals of the cubic unit cell as can be seen in Fig. 3d.

The Ba1 and Ba2 atoms are sitting around this ordered part of the structure (Fig. 4d) and connect this part with the disordered one. Paulus *et al.* (3) have reported that Ba1 and Ba2 lie in the periphery of the six-member ring. However, Ba2 lies exactly in that periphery and the Ba1 atoms are located in the periphery of the BaO_9 polyhedron, as shown in Fig. 4d.

The O1, O2, and O3 atoms form a distorted trigonal prism around Ba1, as shown in Fig. 4a, which is a common polyhedron for Ba with coordination number 9 (14, 15, 16), 8 (15), and 7 (17). The coordination number 7 is not accepted because it leads to an almost perfect trigonal prism (17). The position of Ba1 inside this polyhedron makes more probable (16) the polyhedron with coordina-

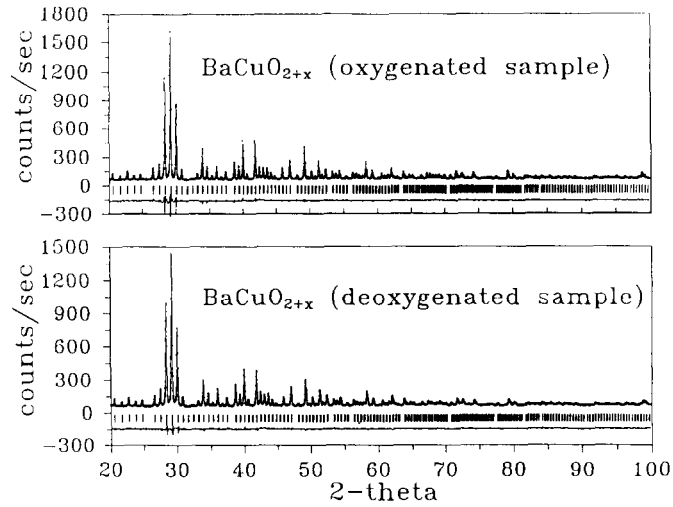

FIG. 2. Rietveld refinement patterns for the samples IIIA (oxygenated) and IIIB (nonoxygenated).

TABLE 2
Bond Lengths for Samples IIIA, IIIB, and the Corresponding Lengths Derived in Previous Structural Studies [Refs. 1–4]

	Sample IIIA	Sample IIIB	Ref. (3)	Ref. (1)	Ref. (2)	Ref. (4)	Ref. (4)
Ba_1–O_1 × 2	2.95(2)	2.95(2)	3.047(9)	2.99	2.99(2)	3.05(3)	3.002(4)
Ba_1–O_2 × 2	2.72(2)	2.78(1)	2.730(7)	2.70	2.72(2)	2.711(4)	2.716(2)
Ba_1–O_3 × 2	2.76(2)	2.74(2)	2.772(9)	2.74	2.78(2)	2.770(5)	2.731(4)
Ba_1–A_2 × 2	—	—	0.794(1)	—	—	—	—
Ba_1–A_4 × 1	2.789(7)	2.792(7)	2.817(4)	2.79	2.78(6)	2.784(4)	2.68(1)
Ba_1–A_7 × 1	—	—	2.950(1)	—	—	—	—
Ba_1–A_8 × 1	2.82(4)	2.85(4)	2.539(1)	2.50	2.73(9)	2.55(1)	2.68(1)
Ba_1–A_9 × 2	3.19(3)	—	3.09(2)	—	—	—	—
Ba_1–A_{10} × 1	—	—	2.187(1)	—	—	—	—
Ba_2–O_2 × 2	2.99(3)	2.83(2)	2.97(1)	2.88	2.85(2)	2.772(4)	2.756(2)
Ba_2–O_3 × 2	3.09(2)	2.87(2)	2.909(9)	2.95	2.95(2)	2.901(3)	2.927(2)
Ba_2–A_6 × 2	—	—	2.793(1)	—	—	—	—
Ba_2–A_8 × 4	2.70(2)	2.78(3)	2.699(1)	2.75	2.76(4)	2.706(5)	2.42(5)
Ba_2–A_9 × 4	2.76(2)	—	2.73(1)	—	—	—	—
Ba_2–A_{10} × 2	—	—	2.806(1)	—	—	—	—
Ba_3–O_1 × 3	2.74(2)	2.78(1)	2.668(7)	2.72	2.66(1)	2.647(6)	2.694(4)
Ba_3–O_2 × 3	3.05(3)	3.17(2)	3.07(1)	3.15	3.18(2)	3.252(5)	3.257(4)
Ba_3–O_3 × 3	2.78(2)	2.89(2)	2.887(9)	2.87	2.89(2)	2.887(3)	2.847(4)
Cu_1–O_2 × 2	1.91(2)	1.87(2)	1.913(7)	1.95	1.94(1)	1.937(4)	1.955(2)
Cu_1–O_3 × 2	1.97(2)	1.97(2)	1.943(9)	1.95	1.91(2)	1.955(3)	1.969(3)
Cu_1–A_9 × 2	2.46(3)	—	2.11(3)	—	—	—	—
Cu_2–O_1 × 4	2.05(2)	2.01(2)	1.999(8)	1.98	1.98(2)	2.00(2)	1.983(2)
Cu_2–A_3 × 2	—	—	1.519(1)	—	—	—	—
Cu_2–A_3 × 4	—	—	2.460(1)	—	—	—	—
Cu_3–O_1 × 4	1.87(2)	1.86(1)	1.958(7)	1.90	1.97(1)	1.948(6)	1.941(2)
Cu_3–A_3 × 4	—	—	2.031(3)	—	—	—	—
Cu_3–A_4 × 1	2.36(5)	2.40(4)	2.38(2)	2.41	2.25(4)	2.44(1)	2.407(7)
Cu_4–A_4 × 1	1.78(5)	1.75(4)	1.81(2)	1.80	1.83(4)	1.93(1)	1.797(7)
Cu_4–A_5 × 1	1.28(2)	1.25(1)	1.220(7)	—	—	—	—
Cu_4–A_6 × 4	—	—	1.825(4)	—	—	—	—
Cu_4–A_7 × 1	—	—	1.249(7)	—	—	—	—
Cu_4–A_8 × 4	1.78(4)	1.76(3)	2.426(9)	2.05	1.72(9)	2.13(1)	1.95(1)
Cu_5–A_8 × 4	2.97(4)	2.97(3)	2.366	—	—	—	—
Cu_5–A_9 × 8	1.43	—	1.75(2)	—	—	—	—
Cu_5–A_9 × 4	—	—	1.712	—	—	—	—

tion number 8. Although the A4 atom is at the right position, the other oxygens that lie opposite to the almost orthogonal plane are missing. The statistically occupied A8 and A9 sites are probably another possible arrangement of oxygen atoms for Ba with coordination number 8. A similar polyhedron is formed around Ba2 by the O2, O3, and Ba2 atoms and the statistically occupied A8 sites (Figs. 4c and 4d). The O2, O3, and Ba2 atoms lie on a mirror plane which produces the mirror image of A8 atoms and another possible orientation for this polyhedron. The atoms at A9 sites are probable oxygen sites for the oxygen atoms not participating in the formation of the distorted trigonal prism around Ba2.

The Cu4, Cu5 atoms and the oxygens named A form the disordered part of the structure and fill the paths between the ordered parts of the structure (Fig. 3d). These paths are parallel to the lines (0.0, 0.5, z) or (x, 0.0, 0.5) or (0.5, y, 0.0), etc. The Cu4, Cu5 atoms are linked through A8 and form chains which are shown in Fig. 4c. The A8 atoms together with A4 form square pyramids around the Cu4. The arrangement of atoms around the Cu5 site (12*d* in Table 1) is more complex.

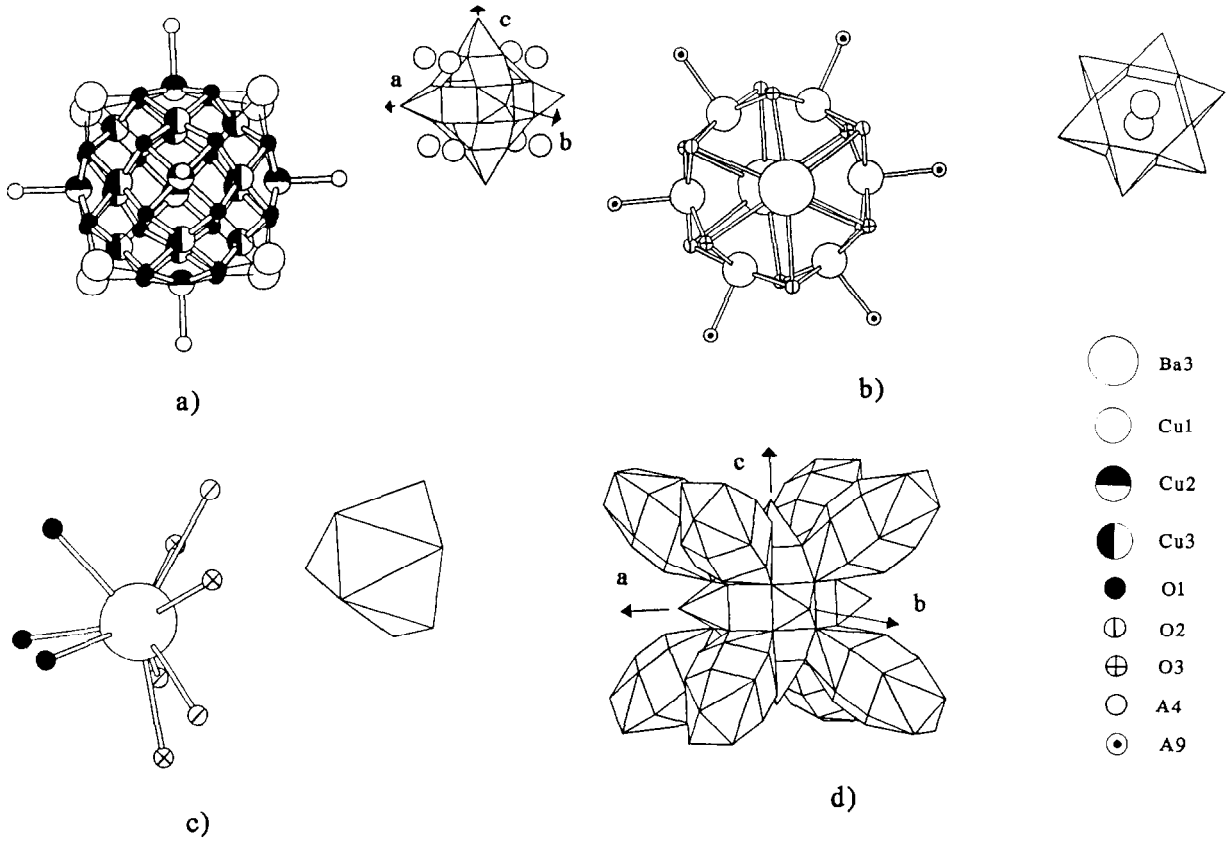

FIG. 3. The ordered part of the crystal structure. (a) The globular and polyhedral models of the $Cu_{18}O_{24}$ polyhedron around the origin (6Cu3, 12Cu2, and 24O1 atoms). The O1 atoms form a square around the Cu2 atom. With the inclusion of A4 atoms, square pyramids are formed around the Cu3 atoms. The Ba3 atoms are bonded with three O1 atoms belonging to this polyhedron. In the polyhedral model the Ba3 atom shows the directions (main diagonals of the cubic cell) along which the ordered part of the structure is developed. (b) The globular and polyhedral models of the six-Cu-member ring Cu_6O_{12} (6Cu1, 6O2 and 6O3 atoms) around the 8*c* site ($\frac{1}{4}, \frac{1}{4}, \frac{1}{4}$) together with the square pyramids formed by the inclusion of the A9 atom. The Ba3 atoms lie above and below this polyhedron along the main diagonal, and each Ba3 atom is connected to six oxygen atoms belonging to this polyhedron. (c) The BaO9 polyhedron around the Ba3 atom in globular and polyhedral representation. Ba3 is connected with 3O1 atoms belonging to the $Cu_{18}O_{24}$ polyhedron and six oxygen atoms (3O2 and 3O3 atoms) of Cu_6O_{12} polyhedron. (d) Connection of the polyhedra that form the ordered part of the structure. The successive order of the polyhedra along each one of the four main diagonals of the cube is $C_{18}O_{24} + BaO_9 + Cu_6O_{12} + BaO_9 + [Cu_{18}O_{24} + BaO_9 \cdots$ (not shown)]. The A9 atoms around the Cu_6O_{12} polyhedron have been suppressed for clarity.

The A8 atoms form a tetrahedron, while the A9 atoms form a square plane. The 12*d* site has been previously assigned to an oxygen atom (1, 2, 4). However, Paulus *et al.* (3) suggested a copper atom for this site, which is in agreement with our results. Attempting a refinement considering this atom site occupied by an oxygen resulted in an occupancy value corresponding to more than one oxygen atom. An overall view of the structure is given by the stereopair picture in Fig. 4d. We believe that the origin for this extremely disordered structure lies in the flexibility of the oxygen atoms to arrange themselves around the Ba and Cu atoms.

In a recent study (18) this compound is identified as an oxocarbonate, with the carbon atom occupying the 12*d* site (Cu5 in our assignment). As was mentioned above, the electron density of this site is higher than the electron density corresponding to an oxygen atom (occupancy factor higher than 1.0 assuming an oxygen atom at this site). Our assignment agrees with the results of (3) and a recent work by Paulus *et al.* (19). It is also worth noting that the oxocarbonate «$BaCuO_2$» sample (18) has been prepared at 850°C, while the samples of the present study have been prepared at temperatures as high as 950°C, thus making the formation of carbon radicals rather unlikely.

In summary, the present study confirms that the 12*d* site is occupied by Cu. It is also shown that the site at the origin (site 2a in Table 1) is more likely to be occupied by oxygen, as it was impossible to refine an atom at this site (4). Additionally, this site was found to be empty in the refinement of the nonoxygenated sample.

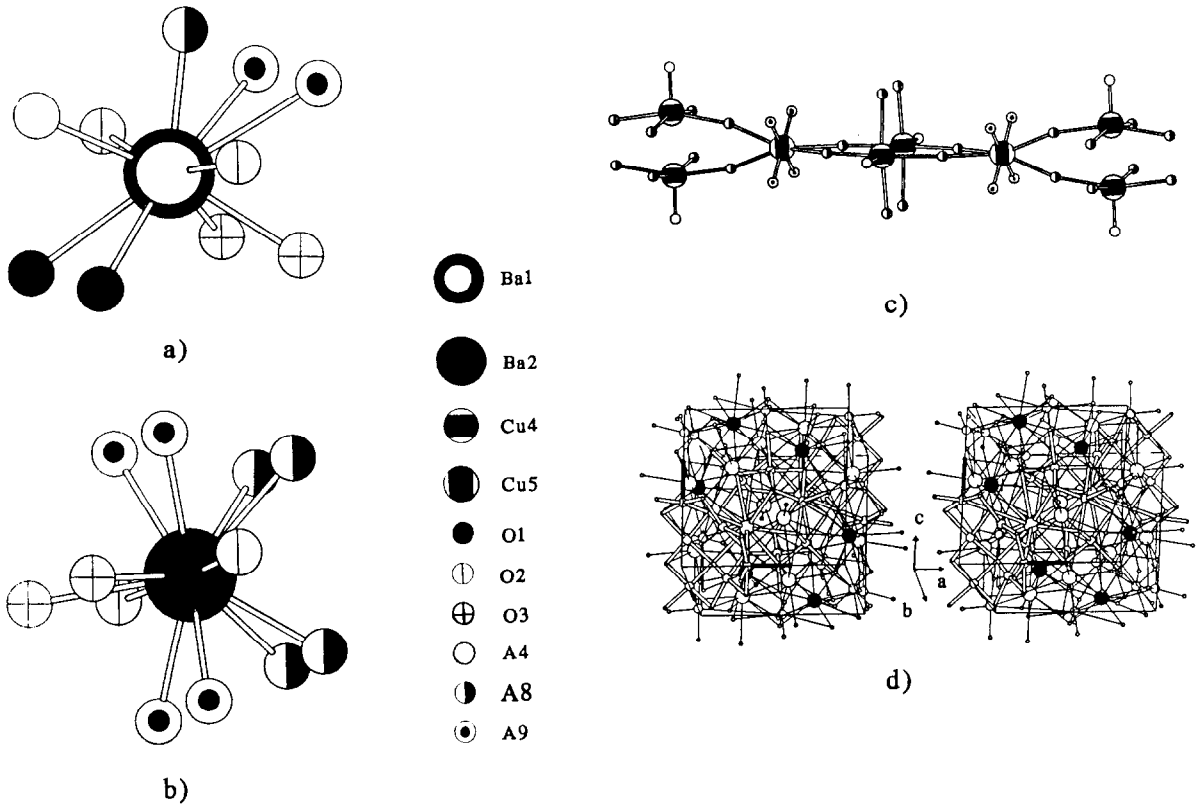

FIG. 4. Description of the disordered part of the structure. (a) The oxygen atom environment of the Ba1 atom. (b) The oxygen atom environment of the Ba2 atom. (c) The Cu4, Cu5 chains along the medians of the cubic surfaces. (d) Stereopair picture of the $\frac{1}{8}$ part of the structure ($\frac{1}{2}$ along each cubic axis) with atoms included. The open bonds connect atoms belonging to the order part. The large circles are Ba atoms (Ba2 atoms are indicated by full black circles). The medium-sized circles correspond to Cu atoms and the small ones to oxygen atoms.

2.3. *Magnetization Measurements*

Magnetic measurements were performed by DC techniques using VSM and SQUID type Quantum Design 5.5T spectrometers in the temperature range from 4.2 K to RT.

The temperature dependence of the inverse susceptibility χ^{-1} for a 1 T magnetic field is shown in Fig. 5 for both phases of sample III. For the oxygenated phase, χ^{-1} vs T curve exhibits a linear temperature dependence above 70 K, which can be described by a Curie–Weiss law $\chi = C/(T - \Theta)$, resulting in a Curie–Weiss constant $\Theta = 15$ K and an effective magnetic moment $\mu_{eff} = 1.89\ \mu_B$/f.u. For the nonoxygenated phase, fitting χ^{-1} vs T to a Curie–Weiss law above 150 K, yields $\Theta = 58$ K and $\mu_{eff} = 1.93\ \mu_B$/f.u. The latter value is higher than $1.82\ \mu_B$, which is expected for divalent copper ions with g = 2.10. The positive values of Θ suggest the presence of ferromagnetic interactions in both phases, though more enhanced in the nonoxygenated one.

As was shown above, the crystal structure of $BaCuO_{2+x}$ comprises an ordered part and a disordered one. The former, which forms the main part of the compound, consists of two structural units, namely, a Cu_6O_{12} ring and a 26-faced $Cu_{18}O_{24}$ polyhedron. Copper ions in the Cu1, Cu2, and Cu3 sites may assumed to be in the divalent state with a predominantly $d(x^2 - y^2)$ ground state due to their square-planar or square-pyramidal coordination. These square-planar units share edges. This geometry according to the superexchange rules (20, 21, 22) is expected to give rise to 90° Cu–O–Cu interactions, which due to the orthogonality of the copper d orbitals will favour ferromagnetic coupling of copper ions in each cluster (10). The short Cu–O bonds (Table 1) are expected to induce strong ferromagnetic intracluster exchange, while weaker intercluster exchange coupling may occur through the disordered part which is formed among the main copper clusters. In this case the magnetic susceptibility should be the result of the contribution of the individual magnetic susceptibilities of both kinds of copper cluster complexes, modified by the weaker intercluster exchange, usually taken into account by a molecular field term (23).

In Fig. 6 the temperature dependence of the effective magnetic moment defined as $\mu_{eff} = 2.83\ (\chi T)^{1/2}$ for χ in emu/mole is presented for both phases. It is seen that the value of μ_{eff} increases upon lowering the temperature from 300 K, reaches a maximum value, and then decreases

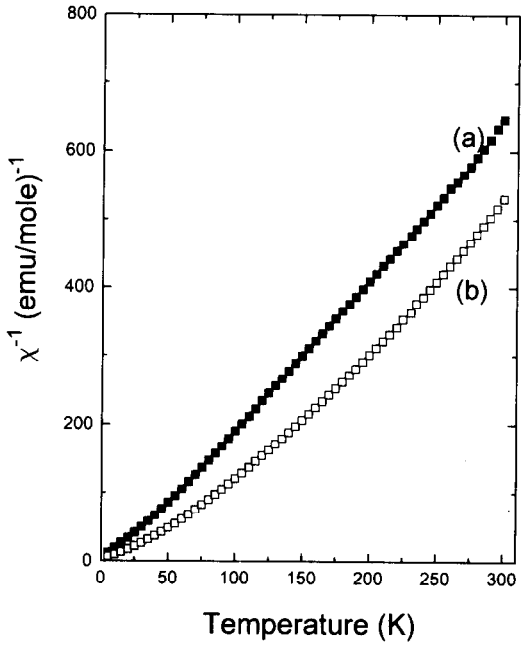

FIG. 5. The inverse magnetic susceptibility as a function of temperature for the (a) oxygenated and (b) nonoxygenated sample III at magnetic field of 1 T.

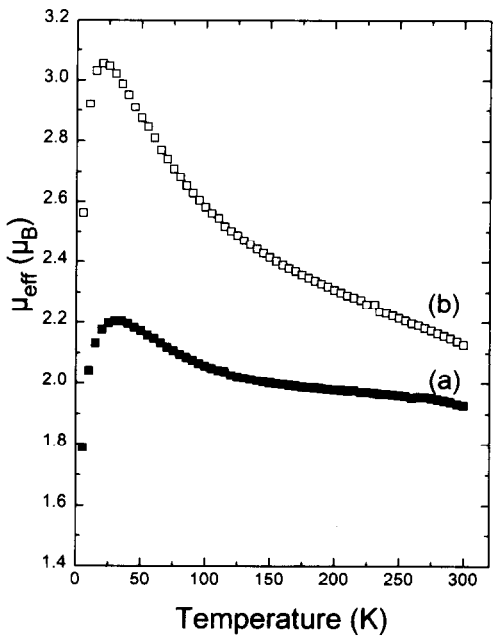

FIG. 6. The effective magnetic moment μ_{eff} as a function of temperature for the (a) oxygenated and (b) nonoxygenated sample III at magnetic field of 1 T.

rapidly. The increase is much more drastic for the nonoxygenated sample. This behaviour is consistent with the presence of the ferromagnetic intracluster interactions and results from the gradual Boltzmann depopulation of the excited states to the cluster ground state which has maximum total spin (24, 25). Considering only isotropic ferromagnetic exchange interaction, the ground state of the Cu_6O_{12} and the $Cu_{18}O_{24}$ cluster complexes will have a total spin 3 and 9, respectively. At low temperatures, taking a typical g value of 2.15, the ground states of these complexes correspond to μ_{eff} values of about 3 and 4.8 μ_B, respectively. The average of these values is slightly larger than the maximum value of μ_{eff} of 3.1 μ_B observed for the nonoxygenated phase, while it is considerably larger than the maximum value of 2.2 μ_B observed for the oxygenated phase (Fig. 6). At low temperatures μ_{eff} exhibits a maximum at a temperature named hereafter as T_{max}, which is equal to 30 and 20 K for the oxygenated and the nonoxygenated phases, respectively. Below T_{max} the value of μ_{eff} decreases rapidly, indicating the predominance of antiferromagnetic intercluster interactions.

The smaller values of μ_{eff} as well as the higher T_{max} observed in the oxygenated phase suggest stronger antiferromagnetic intercluster interactions in this phase. The corresponding curve of Fig. 6 suggests that these interactions are operative in the whole temperature range and not only below T_{max} where they become dominant. This could be expected since the excess oxygen, as was shown by the XRD analysis, occupies vacant sites in the disordered part filling the space among the copper clusters and thus enhances the intercluster antiferromagnetic interactions.

In Fig. 7 the inverse magnetic susceptibility vs T for

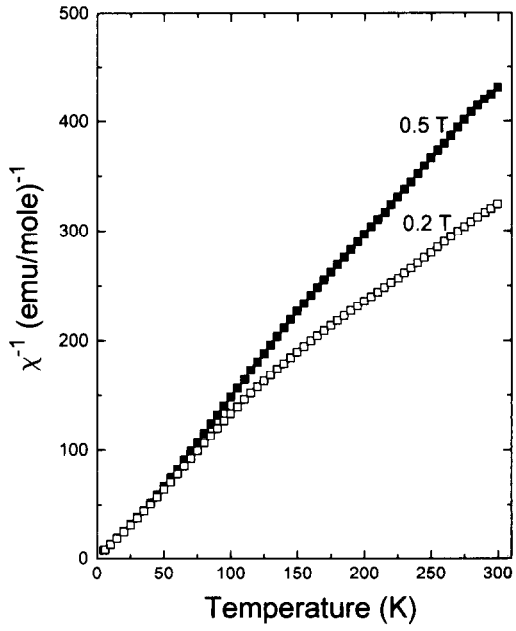

FIG. 7. The inverse magnetic susceptibility χ^{-1} vs T for the nonoxygenated sample III at magnetic fields of 0.2 and 0.5 T.

the nonoxygenated sample III is shown for magnetic fields of 0.2 and 0.5 T. It is seen that the susceptibility is field dependent above 100 K. This behaviour, pending further investigation, might be related to the presence of the large copper clusters and the strong internal fields that they induce in comparison with the externally applied magnetic field. The field dependence of χ might be one of the reasons, besides different oxygen content, that various values of μ_{eff} have been reported in the literature (8, 10, 26).

2.4. *EPR Measurements*

The EPR spectra were recorded by conventional X-band (ν = 9.4 GHz) spectrometers, Bruker ER-200D and Varian E-112, both working with 100 kHz modulation of the steady magnetic field. The Varian E-112 spectrometer was equipped with a reflection double cavity and a static magnetic field varying between 0.025 and 1.0 T. Temperature-dependence measurements were performed using Oxford and Varian systems. The samples (20 mg) in the form of fine powder were placed in quartz tubes of 2 mm diameter. The air from the tube was displaced by flowing He gas.

At RT all samples exhibit a typical powder spectrum of Cu^{2+} ions in orthorhombic local symmetry. The derived spin-hamiltonian parameters are g_x = 2.041(3), g_y = 2.103(3), g_z = 2.223(3) for the oxygenated sample I, and g_x = 2.057(3), g_y = 2.120(3), g_z = 2.21(3) for the nonoxygenated sample I, which are in good agreement with an earlier report (27). However, Cu^{2+} EPR spectra of tetragonal local symmetry such as those reported by Mesquita *et al.* (28), were not observed, probably due to different preparation conditions and oxygen content. The integrated intensity of the observed spectrum corresponds to 2–3% of the total copper concentration as estimated by comparison with the EPR line intensity of $CuSO_4 \cdot 5H_2O$. Based on this observation we assume that this EPR spectrum originates from divalent copper ions in the disordered part of the compound, most probably in the Cu4 and Cu5 sites, which contain only a small fraction of the bulk copper. The local environment of Cu4 consists of a square pyramid, while Cu5 is surrounded by a tetrahedron of A8 oxygen atoms intersected by a square plane of A9 oxygen atoms, which is missing for the nonoxygenated phase (Fig. 4c). The local symmetry of both sites can be further lowered when oxygen atoms in the statistically occupied neighbouring sites are missing, giving rise to the low-symmetry EPR spectra.

The EPR line intensity of this signal is found to be considerably larger, roughly by a factor of 10, in the oxygenated phase compared to the nonoxygenated one for samples I and II, whereas the inverse is found for sample III but with intensities differing only by a factor of 2. Notably, Mesquita *et al.* (28) have reported a clear increase of the EPR line intensity for the deoxygenated samples and, based on this, suggested that removal of oxygen produces the Cu^{2+} resonance. According to the Rietveld analysis of the XRD data, the occupation factors of the two copper sites Cu4 and Cu5 in the disordered part of the crystal structure do not vary considerably with the oxygen content (Table 1). This might indicate that it is the oxygen ordering and not the total oxygen content of the compound which determines the localization of the *d* hole at these copper sites and therefore the strength of the Cu^{2+} signal. Such an explanation may account for the differences observed in the EPR line intensities of the Cu^{2+} spectrum for the various samples which, being prepared under different heat treatment conditions, could have different oxygen distribution in the disordered part. Furthermore, it was found that the intensity of the Cu^{2+} spectrum increased with time in agreement with (28). However, in our opinion this time evolution is most likely related to changes in the oxygen ordering in the disordered part and not to the formation of another compound (28).

For the oxygenated samples, the Cu^{2+} EPR spectrum is observed down to 4 K but below 70 K it is superimposed on another broad line whose amplitude increases rapidly with decreasing temperature (Figs. 8a and 8b). For the nonoxygenated samples the Cu^{2+} spectrum is observed down to 30–40 K (Figs. 9a and 9b) because at lower temperatures it is completely masked by the very intense broad signal. In both cases the superposition of the two different spectra, the Cu^{2+} spectrum and the broad EPR signal, indicates that there is no significant interaction between the corresponding paramagnetic centers. For the nonoxygenated samples which correspond closely to the formula $BaCuO_2$, the broad single EPR line is centered at $g_{eff} \approx 2.15$ for temperatures approximately above 20 K. Its intensity corresponds roughly to that calculated for copper ions in the ordered part of the compound, while the line shape is close to Lorentzian. Due to this observation we ascribe it to the exchange-coupled copper ions in the ordered part.

The intensity J of this EPR signal, estimated by $J = (\Delta H)^2 \cdot I$ at constant modulation and microwave power, with ΔH being the linewidth and I the peak-to-peak amplitude, follows approximately an $\sim 1/T$ law (Fig. 10) in agreement with a previous report (9). This variation complies with the previously described paramagnetic-like behaviour of the DC magnetic susceptibility within the same temperature range, verifying that the EPR signal originates from the copper clusters in the ordered part of the structure. The observation of a single Lorentzian EPR line suggests that exchange narrowing is effective, so that the resonances produced by the two kinds of cluster collapse into a single one. In this case, the intercluster exchange interaction should be larger than the Zeeman energy, which is approximately 0.03 cm^{-1}.

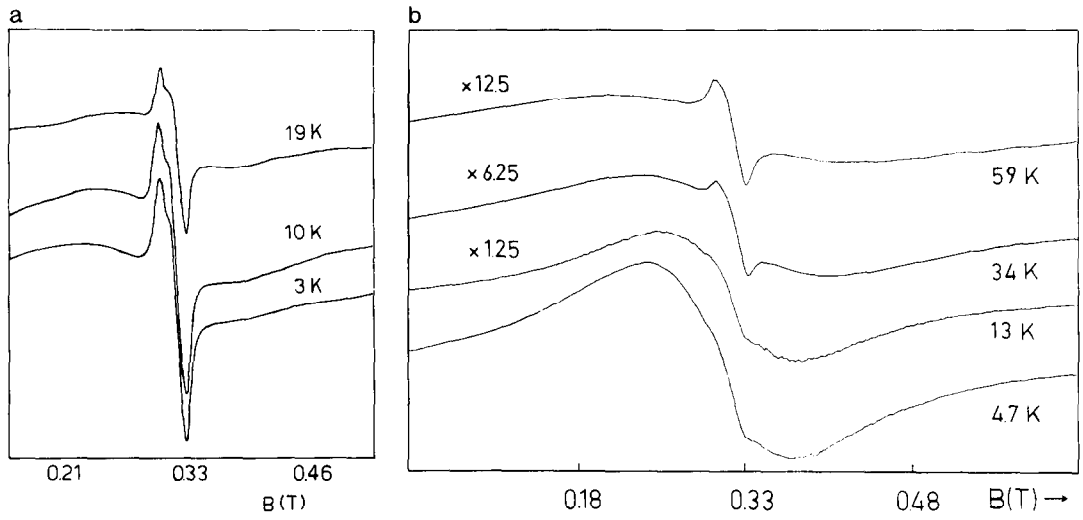

FIG. 8. Temperature dependence of the EPR spectra for the oxygenated (a) sample I and (b) sample III.

The g factor of the EPR line shows a strong temperature dependence below 20 K due to a shift of the resonance line towards lower fields. This can be seen in Fig. 11, where the g factor as a function of temperature is presented for the three nonoxygenated samples. This behaviour can be related to short-range order effects which induce internal fields that add or substract from the external field producing a shift of the resonance line. This effect is consistent with the onset of antiferromagnetic intercluster interactions below 20 K in the nonoxygenated phase as deduced from the magnetic susceptibility measurements. The temperature dependence of the EPR linewidth ΔH is shown in Fig. 12. It is seen that for all samples ΔH exhibits a minimum around 10 K followed by a small increase at lower temperatures. This variation is reminiscent of the divergent behaviour of ΔH due to the slowing down of spin fluctuations when the critical temperature at which long-range order sets in is approached (29). Similar EPR data have previously been reported for samples containing mainly $BaCuO_2$ (8), while specific heat and μSR experiments have detected the presence of magnetic ordering around 11 K (30, 31). Furthermore, fluctuations of the EPR resonance absorption which might be associated with the presence of magnetostatic modes (32) were also recorded around this temperature (Figs. 8a and 8b). All these observations indicate that

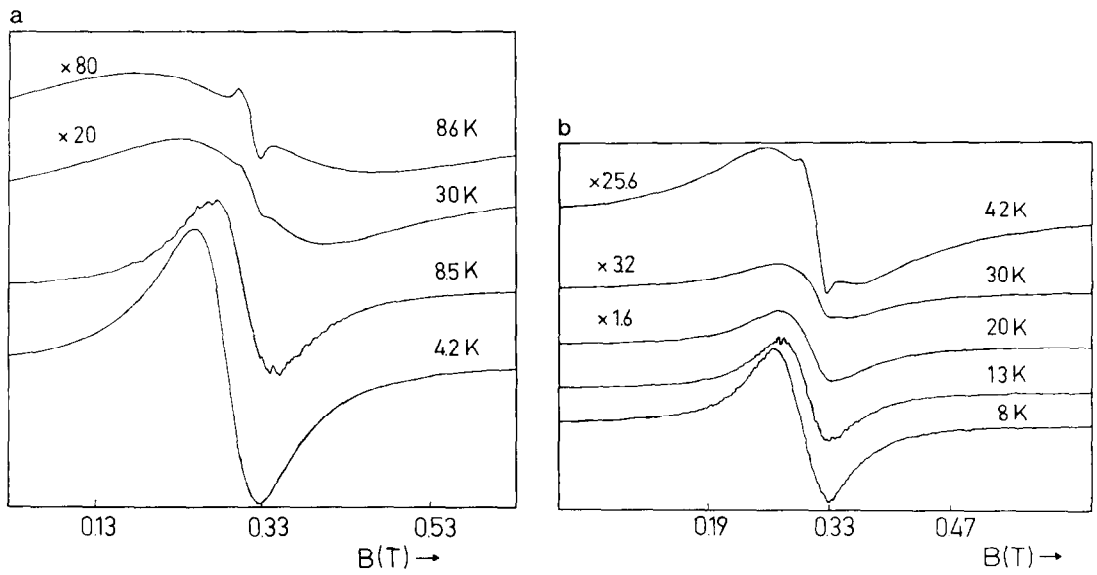

FIG. 9. Temperature dependence of the EPR spectra for the nonoxygenated (a) sample II and (b) sample III.

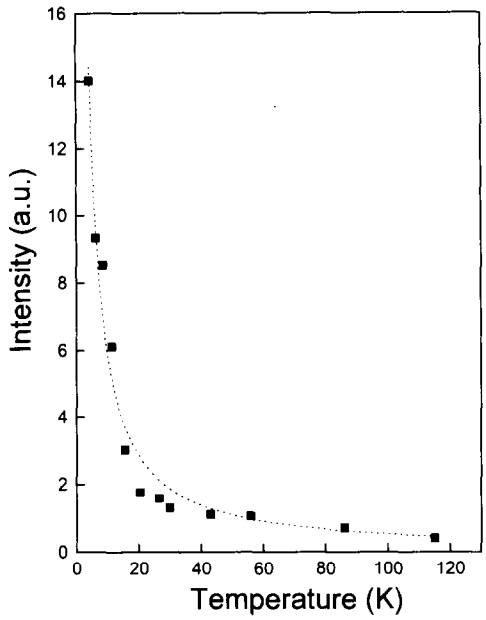

FIG. 10. EPR signal intensity J as a function of temperature for the nonoxygenated sample II. The line represents the best fit curve $\sim T^{-1.04}$.

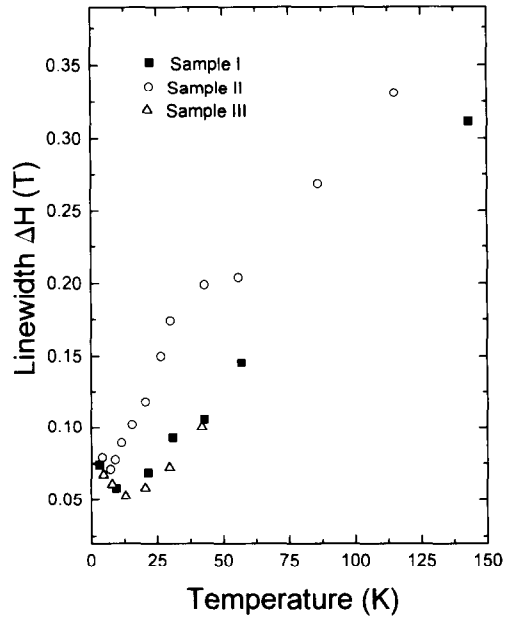

FIG. 12. EPR linewidth ΔH as a function of temperature for the nonoxygenated samples.

antiferromagnetic ordering may occur around 10 K. However, the magnetic susceptibility did not show any critical behaviour around this temperature. The phenomenon should be sensitive to the oxygen content and ordering in the disordered part that provides the pathways for the antiferromagnetic intercluster exchange interactions.

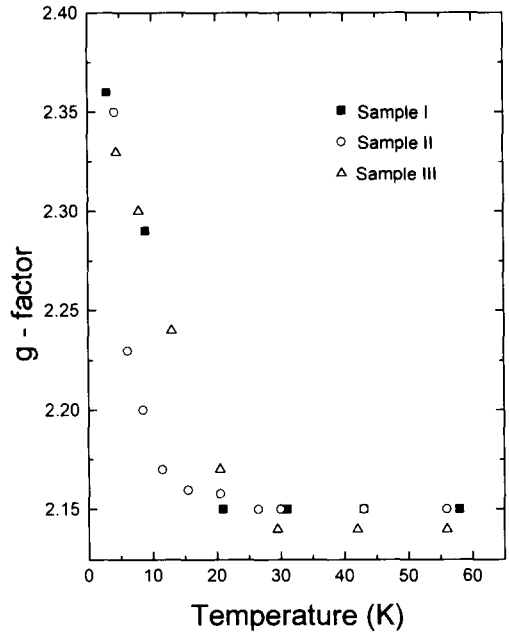

FIG. 11. The g factor of the low-temperature EPR signal as a function of temperature for the nonoxygenated samples.

Neutron diffraction measurements on $BaCuO_{2+x}$ samples with variable oxygen content could possibly clarify this point.

As can be seen in Fig. 12 the EPR linewidth for all samples increases very rapidly with increasing temperature between 20 and ~150 K. Generally, the EPR linewidth for temperatures well above the critical one follows an $1/k_B T\chi$ law, with χ being the static susceptibility, which for strongly correlated systems may be responsible for the temperature dependence of ΔH (33). In the present case, the linewidth increase follows the variation of $1/k_B T\chi$ which also exhibits a sharp, almost linear increase within the same temperature range, as one can easily conclude from Fig. 6. From Fig. 12 it can also be seen that the values of ΔH for the three samples were not identical, indicating a significant effect of heat treatment conditions. Heat treatment most likely affects the oxygen-deficient part of the compound and thus may influence the intercluster exchange coupling which further affects the EPR linewidth.

For the oxygenated samples a similar EPR line is observed (Figs. 8a and 8b) with much broader linewidth, $\Delta H = 0.130(5)$ T at 4.5 K, and intensity an order of magnitude less than that of the nonoxygenated phase. Both observations are related to the reduction of the static susceptibility χ for the oxygenated phase (Fig. 5). The temperature dependence of ΔH for the oxygenated samples (Fig. 13) is qualitatively similar to that of the nonoxygenated ones (Fig. 12) except that the minimum of ΔH is shifted at ~20 K. This observation agrees with the in-

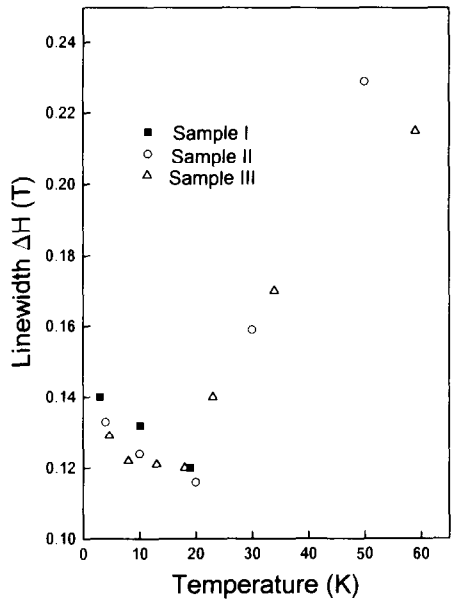

FIG. 13. EPR linewidth ΔH as a function of temperature for the oxygenated samples.

creased value of T_{max} = 20 K of the effective moment of the oxygenated phase (Fig. 6) and also supports the suggestion of stronger antiferromagnetic intercluster interactions in this phase.

Our observations on $BaCuO_2$ seem to be in qualitative agreement with the case of the $Y_2Cu_2O_5$ compound (10, 11, 34). Although the $BaCuO_2$ compound is quite different from the $Y_2Cu_2O_5$ one, mainly due to the presence of the large copper clusters and the existence of a disordered part in its crystal structure, it seems worthwhile to point out the appearance of strong EPR signals corresponding to the bulk copper ions coupled through 90° Cu–O–Cu ferromagnetic interactions in both of them, in contrast with the weak EPR signals observed in compounds with extended 180° Cu–O–Cu antiferromagnetic interactions (10, 11). The reason for not observing any EPR signal in the $BaCuO_2$ material by Shreedhar and Ganguly (10) may be the limited studied temperature region and the different preparation conditions of the samples. We also notice reports that after exposure in air for a few days the XRD pattern and the EPR spectra of $BaCuO_2$ were found to change drastically (35). However, we have not observed either of these effects except for the already mentioned growth of the intensity of the EPR spectra of Cu^{2+} ions.

3. CONCLUSIONS

With this work it was attempted to arrive at a detailed description of the ordered and the disordered part of the crystal structure for the nonstoichiometric compound $BaCuO_{2+x}$, which gives a better understanding of the magnetic properties for this compound.

The magnetic behaviour of the system is determined by the presence of the two kinds of copper clusters, with ferromagnetic intracluster and antiferromagnetic intercluster exchange interactions. The addition of oxygen causes an enhancement of the antiferromagnetic coupling by providing more effective superexchange pathways through the disordered part of the crystal structure. The magnetic susceptibility and the EPR results are consistently described within this picture. From the EPR data there are indications of magnetic ordering at low temperature, in agreement with previous reports of specific heat and μSR experiments. The EPR spectra of Cu^{2+} ions are attributed to copper ions in the disordered part of the compound and appear to depend on the oxygen ordering around these sites.

From the above, it becomes clear that the oxygen atoms in the disordered part of the structure influence the magnetic interactions of the copper atoms. For this reason a systematic study of the structure and magnetic properties of the system based on neutron diffraction data is in progress.

ACKNOWLEDGMENTS

This work was partially supported by the General Secretariat for Research and Technology, Greece, under Grants 89EK19 and 91 EΔ 312.

REFERENCES

1. R. Kipka and H. K. Muller-Buschaum, *Z. Naturforsch* **32b,** 121 (1977).
2. W. Gutau and H. K. Muller-Buschaum, *J. Less-Common Met.* **152,** L11 (1989).
3. E. F. Paulus, G. Miehe, H. Fuess, I. Yehia, and V. Lochner, *J. Solid State Chem.* **90,** 17 (1991).
4. M. T. Weller and D. R. Lines, *J. Chem. Soc. Chem. Commun.*, 484 (1989).
5. J. M. Tranquada, A. H. Moudden, A. I. Goldman, D. E. Cox, G. Shirane, S. K. Sinha, D. Vaknin, D. C. Johnston, M. S. Alvarez, A. J. Jacobson, J. T. Lewandowski, and J. M. Newsam, *Phys. Rev. B* **38,** 2477 (1988).
6. W. E. Farneth, R. S. McLean, E. M. McCarron III, F. Zuo, Y. Lu, R. Patton, and A. J. Epstein, *Phys. Rev. B* **39,** 6594 (1989).
7. H. Gamari-Seale, N. Guskos, A. Koufoudakis, I. Kruk, C. Mitros, V. Likodimos, D. Niarchos, and V. Psycharis, *Philos. Mag. B* **65,** 1381 (1992).
8. D. C. Vier, S. B. Oseroff, C. T. Salling, S. Schultz, Y. Dalichaouch, B. W. Lee, M. B. Maple, Z. Fisk, and J. D. Thompson, *Phys. Rev. B* **36,** 8888 (1987).
9. J. Genossar, D. Shaltiel, V. Zevin, A. Grayevski, and B. Fisher, *J. Phys. Condens. Matter* **1,** 9471 (1989).
10. K. Shreedhar and P. Ganguly, *Inorg. Chem.* **27,** 2261 (1988).
11. P. Ganguly, K. Shreedhar, A. R. Raju, G. Demazeau, and P. Hagenmuller, *J. Phys. Condens. Matter* **1,** 213 (1989).
12. D. B. Wiles and A. R. Young, *Appl. Crystallogr.* **14,** 149 (1981).

13. SHELX76, Program for crystal structure determination, University of Cambridge, England.
14. K. Maroy, *Acta Chem. Scand.* **27,** 1695 (1973).
15. N. O. Persson, H. Wennerstrom, and B. Lindman, *Acta Chem. Scand.* **27,** 1667 (1973).
16. V. H. Mattausch and H. K. Muller-Bauschaum, *Z. Anorg. All. Chem.*, 3861 (1971).
17. H. G. Schnering, *Z. Anorg. Chem.* **314,** 144 (1962).
18. M. A. G. Aranda and J. P. Attfield, *Angew. Chem. Int. Ed. Engl.* **32,** 1454 (1993).
19. E. F. Paulus, G. Wltschek, and H. Fuess, *Z. Kristallogr.* **209,** 586 (1994).
20. J. B. Goodenough, *Phys. Rev.* **100,** 564 (1955).
21. J. B. Goodenough, *Phys. Chem. Solids* **6,** 287 (1958).
22. J. Kanamori, *Phys. Chem. Solids* **10,** 87 (1959).
23. A. P. Ginsberg and M. E. Lines, *Inorg. Chem.* **11,** 2289 (1972).
24. A. P. Ginsberg, *Inorg. Chem. Acta Rev.* **5,** 45 (1971).
25. Y. V. Rakitin, V. T. Kalinnikov, and W. E. Hatfield, *Phys. Status Solidi B* **81,** 379 (1977).
26. R. Troc, Z. Bulowski, R. Horyn, and J. Klamut, *Phys. Lett. A* **125,** 222 (1988).
27. S. K. Hoffmann, B. Czyzak, and J. Stankowski, *Acta Phys. Pol. A* **77,** 621 (1990).
28. R. N. Mesquita, J. H. Castilho, G. E. Barberis, C. Rettori, I. Torriani, O. F. de Lima, S. Gama, R. F. Jardim, M. C. Terrile, H. Basso, and O. R. Nasamento, *Phys. Rev. B* **39,** 6694 (1989).
29. D. L. Huber, *Phys. Rev. B* **6,** 3180 (1972).
30. D. Eckert, A. Junod, T. Graf, and J. Muller, *Physica C* **153–155,** 1038 (1988).
31. A. Weidinger, J. Budnick, B. Chamberland, A. Golnik, C. Nieder-Mayer, E. Recknagel, M. Rossmanith, and De P. Yang, *Physica C* **153–155,** 168 (1988).
32. R. D. Willet and F. Waldner, *J. Appl. Phys.* **53,** 2680 (1982).
33. E. Dormann and V. Jaccarino, *Phys. Lett B* **48,** 81 (1974).
34. B. L. Ramakrishna, E. W. Ong, and Z. Iqbal, *Solid State Commun.* **68,** 775 (1988).
35. J.-T. Yu and K. H. Lii, *Solid State Commun.* **65,** 1379 (1988).